TUDelft

Delft University of Technology

Toward the integrated design of organic rankine cycle power plants

A method for the simultaneous optimization of working fluid, thermodynamic cycle, and turbine

Lampe, Matthias; de Servi, Carlo; Schilling, Johannes; Bardow, Andre; Colonna, Piero

Important note
To cite this publication, please use the final published version (if applicable).
Please check the document version above.

Matthias Lampe[1]
Institute of Technical Thermodynamics,
RWTH Aachen University,
Schinkelstrasse 8,
Aachen 52062, Germany
e-mail: lampe.matthias@googlemail.com

Carlo De Servi[1]
Flemish Institute for Technology Research
(VITO),
Boeretang 200,
Mol 2400, Belgium;
Propulsion and Power,
Aerospace Engineering Faculty,
Delft University of Technology,
Kluyverweg 1,
Delft 2629 HS, The Netherlands
e-mail: carlo.deservi@vito.be or
c.m.deservi@tudelft.nl

Johannes Schilling
Institute of Technical Thermodynamics,
RWTH Aachen University,
Schinkelstrasse 8,
Aachen 52062, Germany
e-mail: johannes.schilling@ltt.rwth-aachen.de

André Bardow
Institute of Technical Thermodynamics,
RWTH Aachen University,
Schinkelstrasse 8,
Aachen 52062, Germany;
Institute of Energy and Climate Research,
Energy Systems Engineering (IEK-10),
Forschungszentrum Jülich GmbH,
Wilhelm-Johnen-Straße,
Jülich 52425, Germany
e-mail: andre.bardow@ltt.rwth-aachen.de

Piero Colonna
Propulsion and Power,
Aerospace Engineering Faculty,
Delft University of Technology,
Kluyverweg 1,
Delft 2629 HS, The Netherlands
e-mail: p.colonna@tudelft.nl

Toward the Integrated Design of Organic Rankine Cycle Power Plants: A Method for the Simultaneous Optimization of Working Fluid, Thermodynamic Cycle, and Turbine

The conventional design of organic Rankine cycle (ORC) power systems starts with the selection of the working fluid and the subsequent optimization of the corresponding thermodynamic cycle. More recently, systematic methods have been proposed integrating the selection of the working fluid into the optimization of the thermodynamic cycle. However, in both cases, the turbine is designed subsequently. This procedure can lead to a suboptimal design, especially in the case of mini- and small-scale ORC systems, since the preselected combination of working fluid and operating conditions may lead to infeasible turbine designs. The resulting iterative design procedure may end in conservative solutions after multiple trial-and-error attempts due to the strong interdependence of the many design variables and constraints involved. In this work, we therefore present a new design and optimization method integrating working fluid selection, thermodynamic cycle design, and preliminary turbine design. To this purpose, our recent 1-stage continuous-molecular targeting (CoMT)-computer-aided molecular design (CAMD) method for the integrated design of the ORC process and working fluid is expanded by a turbine meanline design procedure. Thereby, the search space of the optimization is bounded to regions where the design of the turbine is feasible. The resulting method has been tested for the design of a small-scale high-temperature ORC unit adopting a radial-inflow turbo-expander. The results confirm the potential of the proposed method over the conventional iterative design practice for the design of small-scale ORC turbogenerators. [DOI: 10.1115/1.4044380]

1 Introduction

Organic Rankine cycle (ORC) systems are becoming a consolidated technology for the conversion of low-temperature thermal energy sources (i.e., between $100\,^{\circ}\mathrm{C}$ and $400\,^{\circ}\mathrm{C}$), thanks to their operating flexibility, reliability, scalability, and good efficiency. ORCs are suitable for a wide range of applications [1] such as solar [2] and geothermal [3] power, as well as waste heat recovery from industrial processes [4] or internal combustion engines for heavy-duty trucks [5]. This adaptability to different thermal sources and power capacities stems from the possibility of tailoring the working fluid and the operating conditions of the thermodynamic cycle to the specific application. Thus, the selection of the ORC working fluid represents the key step of the preliminary design procedure of an ORC system [6–8].

In the current design practice, working fluid selection and optimization of the cycle configuration are typically performed successively [2–4,9–12]. First, candidate working fluids are preselected from databases of organic fluids based on the experience of the designer and heuristic knowledge about the application; then, the preselected working fluids are ranked in order of expected process performance. This assessment requires the adaptation of a system model and the solution of an optimization problem to identify the optimal cycle parameters for each working fluid candidate.

To automate and aid these operations, ad hoc high-throughput screening approaches have recently been devised with the aim of rapidly identifying the most promising working fluids from existing large databases [13,14]. However, the outcome of such procedures is arguably highly influenced by the chosen criteria for the preselection of the working fluids. If the criteria do not hold for the application under consideration, suboptimal working fluids are chosen.

To overcome this limitation, alternative methods perform the fluid selection and the thermodynamic cycle design in a more integrated way, as recently reviewed in Refs. [8] and [15]. In pioneering work, Papadopoulos et al. [16] show the merits of a computational framework for computer-aided molecular design (CAMD) of ORC working fluids, whereby the thermodynamic properties of the investigated molecules, which can be already existing but also novel, created in silico, are estimated by a group contribution method. In the first stage, a set of candidate working fluids is obtained by appropriately combining functional groups in a multi-objective optimization problem using process-related performance indicators. In the second stage, the identified candidate working fluids are assessed for the considered ORC process and compared based on the predicted economic performance. In order not to bias the comparison, the ORC parameters are individually optimized for each candidate working fluid.

Bardow et al. [17] presented the continuous-molecular targeting (CoMT) framework for the integrated design of absorption processes, which has been extended to the design of ORC systems by Lampe et al. [18]. In CoMT, the integrated design is achieved by adopting a physically sound model for the prediction of thermodynamic properties of the working fluids: the perturbed-chain statistical associating fluid theory (PC-SAFT) equation of state (EoS) [19]. The pure component parameters of PC-SAFT represent specific physical characteristics of the molecules. In CoMT, these parameters are relaxed to continuous optimization variables in the design problem together with the ORC design parameters. The solution found by the optimizer is a hypothetical optimal working fluid, the so-called target, together with the corresponding optimal ORC configuration. In a second stage, a real working fluid is identified within a fluid database, which shows characteristics similar to the characteristics of the target, through the so-called structure-mapping procedure. For this purpose, a second-order Taylor approximation of the objective function is used to assess real working fluids. To go beyond known databases, novel molecules can be designed using a CAMD formulation based on the group-contribution approach of PC-SAFT [20], by solving the resulting mixed-integer quadratic program in the resulting CoMT-CAMD method [21]. The mapping procedure entails, however, a certain level of approximation, which can lead to poor identification of the optimal molecular structures, as pointed out by Schilling et al. [22]. To overcome such a limitation, the same authors developed the 1-stage CoMT-CAMD [22] method, where the optimal molecule targeting and structure-mapping are simultaneously solved in a single mixed-integer nonlinear programming (MINLP) optimization problem. Thereby, the Taylor approximation and the potential errors caused by the two-stage procedure used by Lampe et al. [18] are eliminated. Schilling et al. [23] complemented the 1-stage CoMT-CAMD method with a model for the prediction of transport properties based on PC-SAFT [24,25]. This information allows for the sizing of the system equipment and the thermo-economic optimization of the ORC unit within the integrated design of the ORC process and working fluid. Recently, the 1-stage CoMT-CAMD method has been extended to multipoint design and optimization by using aggregation techniques [26].

In related work, White et al. [27] proposed a CAMD-based framework for the integrated design of the ORC process and working fluid based on the SAFT γ-Mie EoS [28]. In their method, individual MINLP optimization problems are solved for the hydrocarbon families n-alkanes, methyl alkanes, 1-alkenes, and 2-alkenes. Subsequently, the framework has been extended with

group-contribution models for transport properties allowing the sizing of the equipment [29], and thus the consideration of a thermo-economic objective within the optimization [30]. These studies confirm the suitability of using a SAFT-based thermodynamic model within an integrated design method.

In common design practice of ORC systems, the thermodynamic cycle model used for working fluid selection is generally defined with a fixed value for the isentropic efficiency of the expander [2–4,9–12,16,18,21,31–35]. Only once thermodynamic calculations are completed, the preliminary design of the turbine is performed for the most promising working fluid candidates to assess the technical feasibility of the resulting system and of the expander. The underlying assumption is that turbine efficiency and manufacturability are largely independent of the considered organic working fluid and of the prescribed inlet and outlet operating conditions. This assumption holds well for ORC units with large power output, since the number of stages of the turbine is a degree-of-freedom of the design that can be exploited to overcome the limitations imposed by the manufacturing constraints and to improve the efficiency of the machine. In contrast, this assumption is generally invalid for small power capacity applications, since the number of stages must be as small as possible, preferably one, due to economic reasons and requirements on system compactness. Furthermore, studies on the preliminary design of ORC turbomachinery show that the smaller the power output of the turbine, the more stringent its design constraints and thus the stronger the influence of the working fluid properties on the design and performance of the turbine. For instance, Sauret and Rowlands [36] investigated the performance of a radial-inflow turbine (RIT) with an average rated power of about 300 kW for five working fluids (four refrigerants and n-pentane). They used a well-known meanline code for the preliminary design of radial-inflow turbines and compared the resulting efficiencies and turbine designs. The work shows that the RIT efficiency can vary by a few percentage points depending on the adopted working fluid, i.e., between 75% and 78.5%, but the machine geometry can be completely different. More recently, Bahamonde et al. [37] examined the design of mini-ORC turbines with a power output of 10 kW considering three turbomachinery configurations, namely, radial inflow, multistage radial outflow, and multistage axial. The authors demonstrated that manufacturing and operating constraints reduce the feasible operating envelope of the turbine, hence limiting the maximum cycle pressure and the maximum conversion efficiency of the ORC system. The RIT configuration provides, despite the single stage, the highest design flexibility and adaptability, allowing reaching higher maximum cycle pressure levels.

These results suggest that, especially in the case of the preliminary design of small-capacity ORC power plants, integrating the selection of the working fluids and the optimization of the thermodynamic cycle with the sizing of the turbine is beneficial. For this purpose, in this work, the 1-stage CoMT-CAMD method is enhanced with a turbine meanline model allowing for the integrated design of the ORC process, working fluid, and turbine. The capability and efficiency of the new design method are demonstrated by the design of a high-temperature small-scale ORC unit adopting a radial-inflow turbo-expander.

The paper is structured as follows: the 1-stage CoMT-CAMD method is presented in Sec. 2, together with the submodels for working fluid, process and, turbine preliminary design. The case study is illustrated in Sec. 3. Finally, concluding remarks are given in Sec. 4.

2 The 1-Stage CoMT-CAMD Method for the Design of Working Fluid, Thermodynamic Cycle, and Turbine

As originally presented in Ref. [22], the mathematical problem associated with the integrated design of an ORC process and its working fluid can be formulated as MINLP optimization problem, which reads

$$\max_{x,y^S} f(x,\theta) \tag{1}$$

$$\text{s.t. } g_1(x,\theta) = 0 \tag{2}$$

$$g_2(x,\theta) \leq 0 \tag{3}$$

$$\theta = h(x,z,y^S) \tag{4}$$

$$z = A\,y^S \tag{5}$$

$$F_1\,y^S = 0 \tag{6}$$

$$F_2\,y^S \leq 0 \tag{7}$$

$$x_{\text{lb}} \leq x \leq x_{\text{ub}} \quad \in \mathbb{R}^n \tag{8}$$

$$0 \leq y^S \leq y^{S,\max} \quad \in \mathbb{N}^m \tag{9}$$

The evaluation of the objective function f requires a process model of the ORC system, which is represented by the equality constraints g_1 and inequality constraints g_2 in Eqs. (1)–(3). The model inputs are the equilibrium thermodynamic properties of the working fluid θ (e.g., the fluid enthalpy at the different cycle states), and the process variables x (e.g., the pressure levels or the mass flow rate of the working fluid). The previous version of 1-stage CoMT-CAMD employed a process model for the ORC cycle with a constant efficiency for the expander. In this work, the set of constraints g_1, g_2 includes also a preliminary design model for a radial inflow turbine. The specific functional form of the problem constraints is shown in Secs. 2.2 and 2.3. The thermodynamic properties θ are computed in Eq. (4) using the physically based PC-SAFT equation of state [19] as a function of the process variables x and of the pure component parameters z. The pure component parameters z, in turn, are determined in Eq. (5) by using a group-contribution method of PC-SAFT [20] based on the molecular structure of the working fluid y^S, as explained in Sec. 2.1. y^S is a vector where each entry y_i^S represents the number of occurrences of the functional group i in the molecular structure of the working fluid. Finally, the linear equality and inequality constraints in Eqs. (6) and (7) enforce the structural feasibility of the molecule (e.g., no open bonds, for details see Ref. [38]).

The MINLP in Eqs. (1)–(9) is solved in 1-stage CoMT-CAMD by an outer-approximation algorithm combined with a relaxation strategy, as implemented in the local MINLP solver DICOPT [39]. More specifically, a relaxed MINLP problem is initially solved, where all integer variables are allowed to take on continuous values. The relaxed MINLP results in a hypothetical, optimal working fluid, the so-called target, which serves as an upper bound of the mixed-integer optimization problem and corresponds to the solution of the CoMT problem in the two-stage CoMT-CAMD approach [18]. Subsequently, a feasible molecular structure is identified based on the target. To solve the optimization problem, the software GAMS (version 24.7.3) is used. However, to ensure the convergence of the calculations, the process and thermodynamic properties model (PC-SAFT equation of state) are implemented in a dedicated and separate code, which is interfaced to GAMS.

A single objective function is here considered, although multi-objective optimization can be also employed in order to capture trade-offs between different performance indicators and their relation to the various molecular structures [22]. The figure of merit to compare the working fluids can be the net power output of the ORC unit P_{net} or its conversion efficiency η depending on the specific ORC application under consideration. Furthermore, a thermo-economic objective can be also considered if a model for transport properties of the working fluid is adopted together with a preliminary design procedure for the main system equipment [23].
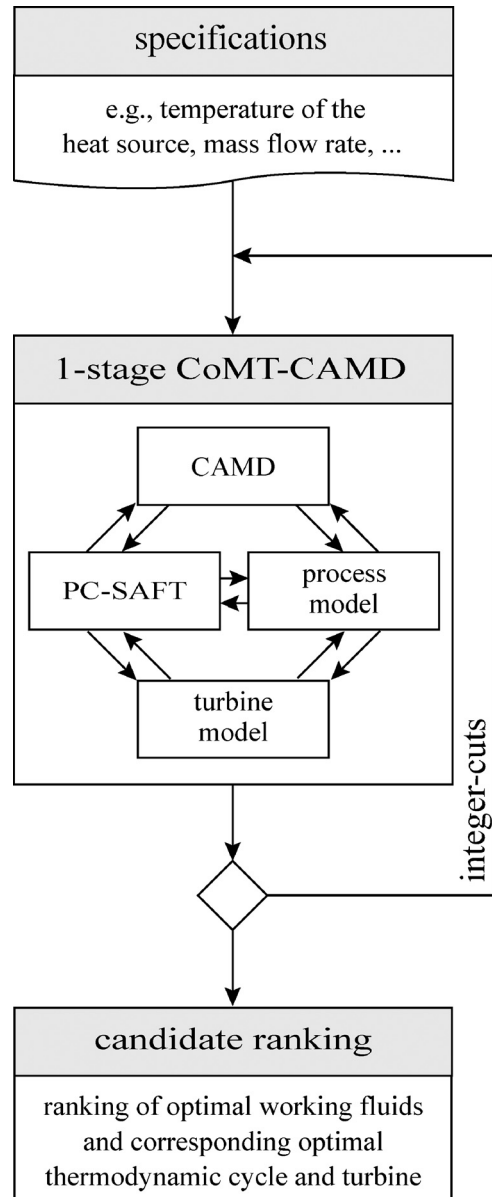

Fig. 1 Workflow of the 1-stage CoMT-CAMD method for the integrated design of working fluid, ORC process, and turbine [22]

To take model inaccuracies into account and to prevent local optimal solutions, the outcome of CAMD methods is usually a list of candidate fluids. However, the solution of the single-objective optimization problem in Eq. (1)–(9) is a sole organic working fluid, either existing or new, and the corresponding optimal thermodynamic cycle and turbine. The MINLP is, thus, solved repeatedly for a given number of times selected by the designer, wherein the previous solutions are excluded from the feasible design space by using integer cuts [40]. To reduce computation effort, the solution of the relaxed MINLP is saved and set as the initial value for all subsequent MINLPs. The resulting overall design workflow is shown in Fig. 1.

With respect to the work in Ref. [22], the ORC process model integrates a method for preliminary design of radial-inflow turbines. The aim is (i) to evaluate the primary characteristics of the machine, such as the velocity triangles, the speed of revolution, and the main blading geometrical parameters, (ii) to estimate the expander efficiency, and (iii) to discard the combinations of working fluid and cycle configurations that would lead to unfeasible turbine designs. As per conventional practice in turbomachinery preliminary design [41], the method is based on a 0D meanline model for the expander, which is presented in Sec. 2.3.

2.1 Working Fluid Model. The thermodynamic model of the working fluid is based on the PC-SAFT equation of state. PC-SAFT is a model for the residual Helmholtz energy and thus gives a thermodynamically consistent prediction of the thermo-physical equilibrium properties of fluids. More specifically, a molecule is modeled as a perturbed chain of spherical segments, whose structure is described by a set of typically 3–7 pure component parameters. In this work, only nonquadrupolar working fluids are considered. Thus, six pure component parameters are needed to describe a molecule. Two of these parameters are geometric: the number of segments m and the segment diameter σ. The magnitude of the interaction forces between the chain segments is captured by the segment dispersion energy (ε/k) and the dipole interaction by the dipole moment μ. The associating interaction is characterized by the associating energy $\varepsilon^{A,B}$ and the associating volume $\kappa^{A,B}$. For a detailed description of the PC-SAFT EoS, the reader is referred to the original literature [19,42,43].

The pure component parameters $z = (m, \sigma, (\varepsilon/k), \mu)^T$ of PC-SAFT are generally fitted to thermodynamic data, if available. This clearly cannot be the case for molecules created in silico. Here, the pure component parameters are, thus, predicted by using the homosegmented group-contribution method from Sauer et al. [20]. According to this method, the molecular structure of the working fluid is decomposed into smaller structural elements, the so-called functional groups. Each functional group provides a specific contribution to the pure component parameters z. The pure component parameters z are estimated by assuming group additivity. The relation between the pure components parameters z and those associated with each functional group, thus, reads [20]

$$m = \sum_{i \in I} y_i^S \cdot m_i \tag{10}$$

$$m \sigma^3 = \sum_{i \in I} y_i^S \cdot m_i \cdot \sigma_i^3 \tag{11}$$

$$m \frac{\varepsilon}{k} = \sum_{i \in I} y_i^S \cdot m_i \cdot \left(\frac{\varepsilon}{k}\right)_i \tag{12}$$

$$\mu = \sum_{i \in I} y_i^S \cdot \mu_i \tag{13}$$

$$\varepsilon^{A,B} = \sum_{i \in I} y_i^S \cdot \varepsilon_i^{A,B} \tag{14}$$

where the vector y^S accounts for the number of occurrences of each functional group i in the molecular structure of the working fluid. Due to the strong interaction between the associating pure component parameters, we do not calculate the associating volume $\kappa^{A,B}$ from group contributions, but we set $\kappa^{A,B} = 0.03$ if a group with $\varepsilon^{A,B} > 0$ is selected. For $\kappa^{A,B} = 0.03$, the group contribution of the associating energy is adjusted to $\varepsilon_{OH}^{A,B} = 2025.0$ K for 1-alcohols and to $\varepsilon_{NH_2}^{A,B} = 1033.7$ K for 1-amines. The groups considered in this work allow for the design of branched and unbranched alkanes ($-CH_3$, $-CH_2-$, $>CH-$, $>C<$), alkenes ($=CH_2$, $=CH-$, $>C=$), 1-alkynes ($-C\equiv CH$), hexane rings ($>CH^{Hex}-$, $/CH_2^{Hex}-$), pentane rings ($>CH^{Pent}-$, $/CH_2^{Pent}-$), aromatics ($>C^{Arom}=$, $/CH^{Arom}=$), aldehydes ($-CH=O$), ketones ($>C=O$), ethers ($-O-CH_3$, $-O-CH_2-$), esters ($-O-(C=O)-$) and formates ($-O-CH=O$), 1-alcohols ($-OH$), and 1-amines ($-NH_2$). In ring molecules, only one ring is allowed and only alkyl side chains are considered. The extension to an even broader set of molecular groups is straightforward if the corresponding parameters for the calculations in the group-contribution method are known. For molecular families that are not covered by the group contribution method proposed by Sauer et al. [20], the needed group contribution parameters have to be first adjusted to measurement data. Unfortunately, the functional

groups for siloxanes are not yet available such that this important class of working fluids has to be excluded from our analysis. In this work, we therefore consider both hexamethyldisiloxane (MM) and octamethyltrisiloxane (MDM) as benchmark fluids.

For caloric properties, the PC-SAFT EoS is complemented by a model for the ideal gas heat capacity c_p^{ig} of the organic working fluid. In the previous works of Lampe et al. [18,21] and Stavrou et al. [44], a custom-made quantitative structure–property relationship model was adopted. In this work, the estimate of c_p^{ig} is performed by using the group contribution method from Joback and Reid [45]. Consequently, all thermodynamic equilibrium properties of the working fluid are predicted starting from its molecular structure.

The presented CAMD scheme does not discriminate among the candidate working fluids based on non-thermodynamic properties such as toxicity, flammability, global warming potential, or thermal stability. All of these properties that can be predicted by group contribution methods [16,34] can directly be taken into account in the CAMD formulation, e.g., by introducing proper constraints into the optimization problem. However, in this work, non-thermodynamic properties are assessed only a posteriori for the sole top-ranked working fluids, based on literature data. The reason is that solutions characterized by working fluids that are not fully satisfactory in terms of environmental or safety requirements can still be attractive [46]. For instance, a working fluid enabling high conversion performance, but flammable, can still be the optimal choice if appropriate measures to guarantee system safety can be employed. The additional investment costs with respect to a solution with a nonflammable fluid might be compensated by the larger amount of converted energy of the plant or by the smaller size of the equipment.

2.2 Process Model. For demonstrative purposes, a single-pressure recuperated thermodynamic cycle configuration is considered. With reference to Fig. 2(a), the working fluid leaves the primary heat exchanger (PHE) of the system at state 1 as saturated or superheated vapor and is then expanded from state 1 to state 4 in a 90 deg radial-inflow turbine. Afterward, the working fluid enters the recuperator and is cooled to state 5. The working fluid becomes liquid in the condenser and it is saturated at its outlet (state 6). Then, the fluid is extracted from the condenser by the pump and circulated back into the high-pressure part of the ORC loop. Before entering the primary heat exchanger, the pressurized working fluid is preheated in the recuperator from state 7 to 8. Constant pressure drops in the heat exchangers are assumed. The cooling fluid in the condenser is assumed to be ambient air (state C1). The air enters the condenser propelled by fans in state C2. At the outlet of the tube banks, the air is in state C3. The air flow rate $\dot{m}_{air}$ is calculated on the basis of the minimum temperature difference assumed in the condenser.

In general, a recuperated ORC proves to be the most appropriate cycle configuration to assess different working fluids with an automated methodology. First, the recuperated ORC exhibits better thermodynamic performance than the simple cycle arrangement for both waste heat recovery and conversion of primary energy sources. Second, more complicated cycle configurations, such as multipressure level or cascaded cycles, are seldom adopted to limit capital expenditures. In the case of primary energy sources, the recuperator allows for increasing the average temperature at which thermal energy is fed to the ORC turbogenerator, thus boosting the cycle efficiency. For waste heat recovery, internal recuperation has either no impact or a positive effect on the ORC power output, despite the reduced amount of thermal energy recovered, as demonstrated in Ref. [47]. In both types of applications, the adoption of a recuperated cycle configuration, thus, allows the identification of the solutions with the highest net power output.

The process variables x that serve as degrees-of-freedom of thermodynamic cycle optimization are: the reduced pressure at
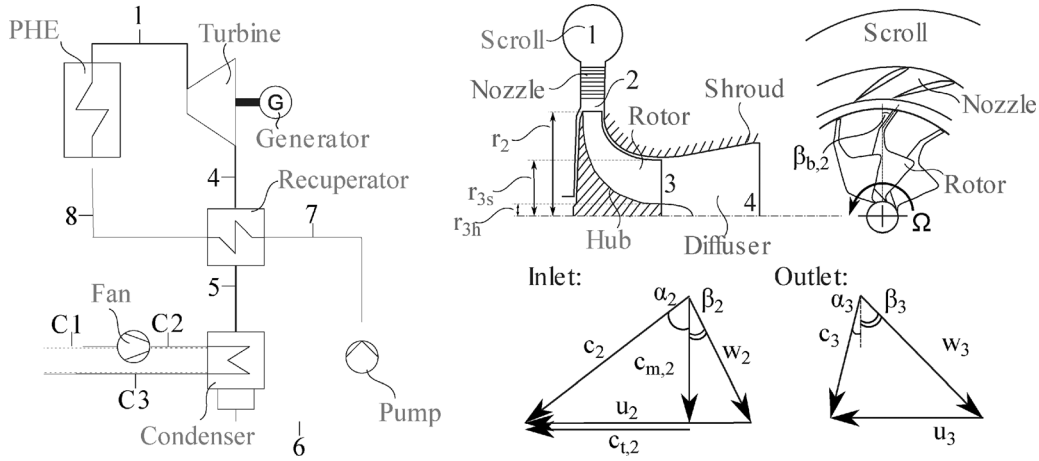
Fig. 2   A schematic of process (left) and radial turbine including the corresponding velocity triangles (right)

the primary heat exchanger and condenser outlet, respectively $p_{\text{out,PHE}}$ and $p_{\text{out,cond}}$, the working fluid mass flow rate $\dot{m}_{\text{wf}}$, and the degree of superheating of the vapor at state 1 ΔT_{sh}. The thermodynamic cycle design is subject to the inequality constraints g_{process} with

$$g_{\text{process}} = \begin{pmatrix} (\dot{m}_{\text{wf}}\,(h_1 - h_8) - \dot{Q}_{\text{PHE}}^{\max}) \\ T_1 - T_{\text{PHE}}^{\text{out,max}} \\ T_{\text{cond}}^{\min} - T_6 \\ \Delta T_{\text{cond}}^{\min} - T_5 + T_{C3} \\ \Delta T_{\text{cond}}^{\min} - T_6 + T_{C2} \\ \Delta T_{\text{regen}}^{\min} + T_8 - T_4 \\ \Delta T_{\text{regen}}^{\min} + T_7 - T_5 \end{pmatrix} \leq 0 \qquad (15)$$

The inequality constraints g_{process} (Eq. (15)) involve the maximum amount of thermal energy transferred into the process $\dot{Q}_{\text{PHE}}^{\max}$, maximum cycle temperature $T_{\text{PHE}}^{\text{out,max}}$, minimum condensation temperature $T_{\text{cond}}^{\min}$, and minimum temperature difference in the heat exchangers $\Delta T^{\min}$. The procedure to calculate the thermodynamic cycle states and power output is not reported here since it is performed according to the standard sequence which can be found in engineering thermodynamics textbooks, see, e.g., Ref. [48].

2.3   Turbine Model. Within the proposed 1-stage CoMT-CAMD method, the turbine preliminary design is primarily aimed at verifying the technical feasibility of a RIT given the outputs of thermodynamic cycle calculations, namely, the fluid mass flow rate, the thermodynamic state at the inlet of the expander, and the expansion ratio. The meanline model used for this purpose is based on the seminal work of Glassman [49] and Baines [50], as well as on previous studies of some of the authors on the preliminary design of radial-inflow mini-ORC turbines [37,51].

The technical feasibility of the turbine is ensured by introducing inequality constraints in Eq. (3), which account for the geometrical, fluid-dynamic, and technical limitations associated with turbine design and operation. These inequality constraints are defined as g_{turb} with

$$g_{\text{turb}} = \begin{pmatrix} b_2^{\min} - b_2 \\ \Omega - \Omega^{\max} \\ M_{\text{w,2}} - M_{\text{w,2}}^{\max} \\ b_3/b_2 - (b_3/b_2)^{\max} \end{pmatrix} \leq 0 \qquad (16)$$

The constraints g_{turb} (Eq. (16)) bound the minimum blade height at the rotor inlet $b_2^{\min}$, the maximum rotational speed of the

turbine $\Omega^{\max}$, and the relative Mach number at the rotor inlet $M_{\text{w,2}}^{\max}$. Additionally, an upper limit is set on the inlet to outlet blade height ratio of the impeller $(b_3/b_2)^{\max}$ to avoid excessive volumetric flow ratios across the turbine, which are known to be detrimental for the efficiency of the machine [52]. The selected design variables are the nozzle and rotor blade angles $\alpha_{\text{b,2}}$, $\beta_{\text{b,2}}$, and $\beta_{\text{b,3}}$, the outlet hub to shroud radius ratio $r_{\text{h,3}}/r_{\text{s,3}}$, the outlet shroud radius to inlet radius ratio $r_{\text{s,3}}/r_2$, and the isentropic reaction degree R_{s}.

The prediction of the turbine performance requires modeling the main loss mechanisms over the expansion process. In this work, as common in practice, the fluid-dynamic losses are assumed to be a function of the kinetic energy of the fluid at the nozzle outlet, i.e.,

$$h_2 - h_{2,\text{s}} = \frac{1}{2}\,\zeta_{\text{n}}\,c_2^2 \qquad (17)$$

where ζ_{n} is the nozzle enthalpy loss coefficient, while the subscript "s" indicates the state resulting from an isentropic expansion process. Typical values of ζ_{n} reported in the literature for conventional radial-inflow turbines are in the range of 0.05–0.1. It results, then, that the turbine efficiency is marginally affected by nozzle performance [53]. In the case of radial-inflow ORC turbines, the influence of the nozzle on overall expansion efficiency is expected to be greater due to the highly supersonic conditions at the stator outlet, which arise from the high expansion ratio of the turbine, if compared to traditional air/gas machines, and the low speed of sound typical for organic working fluids. This effect is confirmed by Bahamonde et al. [37] for radial-inflow turbines operating with working fluids of high molecular complexity. Their predictions show that (i) more than 50% of turbine losses are generated in the stator, and (ii) half of the nozzle losses are due to the mixing out losses in the supersonic flow beyond the trailing edge. However, the value of ζ_{n} calculated for different design solutions is found to vary only slightly with pressure ratio and the Mach number M_2, even for values of M_2 close to 2. This lack of correlation between ζ_{n} and the expansion ratio is due to the adoption of a converging-diverging profile for nozzle blades if $M_2 > 1.4$. Such a design solution, common in ORC turbines [54], allows limiting the losses in the supersonic expansion for operation around the nominal design point even in case of high nozzle pressure ratios and Mach numbers. Hence, to a first approximation, the nozzle enthalpy loss coefficient ζ_{n} is here taken constant regardless of the characteristics of the working fluid under consideration. Coherently with this assumption, the deviation between the flow direction and the blade angle at the nozzle outlet is neglected.

Fluid-dynamic losses in the rotor are predicted according to well-established loss correlations [50], which account for three main dissipative effects: friction, secondary flow, and tip leakage.

Incidence and windage losses are considered negligible. Incidence losses are neglected assuming that the rotor is designed with an optimum back swept inlet angle such that perfect incidence for the incoming flow is attained; windage losses are not considered in the model because their contribution seems to be irrelevant according to recent measurements in an ORC centripetal expander [55]. Moreover, in analogy with the stator, flow deviations from the blade angle at the rotor outlet are ignored, and kinetic energy recovery in the diffuser is neglected as per common practice in the preliminary design of ORC turbines [36,37,51,56]. The fluid thermodynamic conditions at turbine outlet, namely, at state 4 in Fig. 2, are then taken equal to those of state 3, i.e., at the rotor outlet.

With these assumptions, the calculation scheme of the meanline code is as follows:

(1) First, the values of geometric parameters such as the rotor inlet flow angle β_2 and the number of rotor blades of the turbine are precomputed based on the model inputs. The rotor inlet flow angle β_2 is estimated by using Wiesner's correlation for slip factor in centrifugal impellers [57], after proper adaption for turbines [58], whereas the optimum number of blades is determined by applying the criterion of Glassman reported in Ref. [49].

(2) The isentropic enthalpy resulting from an ideal expansion through the nozzle, i.e., $h_{2,s}$ in Fig. 3, is calculated on the basis of the total inlet conditions, the outlet pressure, and the reaction degree of the turbine. From the definition of the reaction degree of the turbine, the isentropic enthalpy $h_{2,s}$ is given by

$$h_{2,s} = h_{3,ss}(p_3, s_1) + R_s \cdot (h_1(p_1, T_1) - h_{3,ss}(p_3, s_1)) \tag{18}$$

Once $h_{2,s}$ is known, the intermediate pressure between nozzle and rotor p_2 can be evaluated.

(3) The stator outlet velocity c_2 is estimated by solving the energy balance for the stator. Notably, combining the conservation of total enthalpy with Eq. (17) yields

$$c_2 = \sqrt{2 \cdot (h_{01} - h_{2,s})/(1 + \zeta_n)} \tag{19}$$
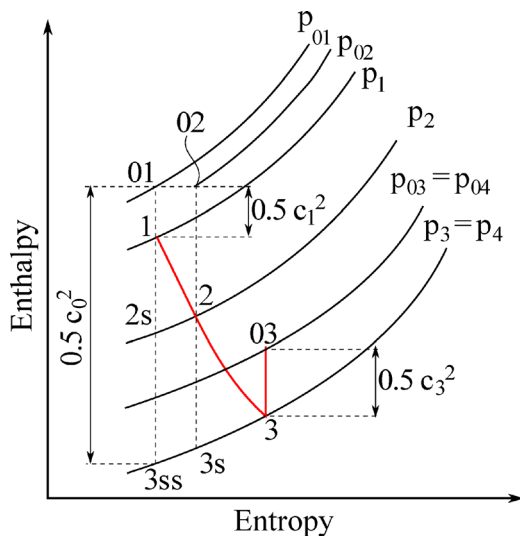
Fig. 3 Enthalpy–entropy chart of the expansion process in the turbine. The flow enters the turbine in state 1 (Fig. 2), passes through the nozzle, and enters the rotor in state 2. The fluid leaves the rotor in state 3 and exits the turbine also in state 3 as the effect of the diffuser is neglected. The subscript "0" before the state number denotes total thermodynamic conditions.

where the subscript "0" before the station point number indicates total thermodynamic conditions. Since the flow angles α_2 and β_2 are known, the corresponding velocity triangle at the rotor inlet can be determined by simple trigonometric relations. Moreover, by means of Eq. (17), it is now also possible to estimate the actual static enthalpy h_2 of the fluid at the nozzle outlet, thereby fully characterizing the thermodynamic state at the stator outlet.

(4) The peripheral speed at the rotor outlet u_3 is given by the following geometric relation:

$$u_3 = \frac{r_3}{r_2} u_2 = \frac{1}{2} \frac{r_{s,3}}{r_2} \left(1 + \frac{r_{h,3}}{r_{s,3}} \right) u_2 \tag{20}$$

(5) The thermodynamic conditions and the velocity triangle at the rotor outlet are determined by solving a nonlinear system of equations through an iterative procedure. In contrast to the assumption at the basis of the nozzle submodel, namely that the loss coefficient is constant, the prediction of the rotor losses originates from empirical correlations, which require knowledge of the shape and main dimensions of the impeller blade channels. These geometric inputs, such as the blade chord, can be expressed as a function of the blade height and the mean radius at the inlet and outlet section of the rotor, see Ref. [50]. These quantities, in turn, can be estimated once the fluid thermodynamic conditions and velocity at State 3 are given. The modeling of the expansion process across the rotor, thus, entails the solution of the equivalent equation system in the unknowns $b_2, r_2, b_3, r_3, \zeta_r, h_3$, and w_3

$$\begin{cases} h_2 + \dfrac{w_2^2}{2} - \dfrac{u_2^2}{2} = h_3 + \dfrac{w_3^2}{2} - \dfrac{u_3^2}{2} & (21a) \\[2mm] h_3 - h_{3,s}(p_3, s_2) = \zeta_r \dfrac{w_3^2}{2} & (21b) \\[2mm] \zeta_r = f(b_2, b_3, r_2, r_3) & (21c) \\[2mm] r_2 = \sqrt{\dfrac{\dot{m}_{wf}}{\pi \rho_3(p_3, h_3) w_3 \cos\beta_3 \left(\dfrac{r_{s,3}}{r_2}\right)^2 \left[1 - \left(\dfrac{r_{h,3}}{r_{s,3}}\right)^2\right]}} & (21d) \\[4mm] b_2 = \dfrac{\dot{m}_{wf}}{2\pi r_2 \rho_2 c_2 \cos\alpha_2} & (21e) \\[2mm] r_3 = \dfrac{1}{2}\left(\dfrac{r_{s,3}}{r_2}\right)\left[1 + \left(\dfrac{r_{h,3}}{r_{s,3}}\right)\right] r_2 & (21f) \\[2mm] b_3 = \left(\dfrac{r_{s,3}}{r_2}\right)\left[1 - \left(\dfrac{r_{h,3}}{r_{s,3}}\right)\right] r_2 & (21g) \end{cases}$$

Equation (21a) implements the conservation of rothalpy, while the expression for b_2 and r_2 results from applying the conservation of mass at the impeller inlet and outlet sections. Equation (21f) expresses the geometric relation between the inlet and outlet rotor diameter as a function of the design variables $r_{h,3}/r_{s,3}$ and $r_{s,3}/r_2$. Similarly, Eq. (21g) represents the geometric relation between the blade height at the rotor outlet b_3 and the inlet rotor diameter r_2. Notice also in Eq. (21b) the definition of the loss coefficient ζ_r. Its value depends on the empirical correlations in Ref. [50], here synthetically represented by the implicit relation (21c).

(6) Finally, the model outputs of interest, i.e., the turbine isentropic efficiency η_s, the rotational speed Ω, and the Mach number at the rotor inlet $M_{w,2}$ are calculated as

$$\eta_s = \frac{h_{01} - h_{03}}{h_{01} - h_{3ss}} \tag{22}$$

Table 1 Parameter assumed for the ORC process model of the case study

Parameter	Symbol	Value
Turbine		
Generator efficiency	η_{gen}	0.95
Minimum blade height	b_2^{min}	2 mm
Maximum rotational speed	Ω^{max}	70,000
Maximum Mach number	M^{max}	0.9
Maximum outlet to inlet blade height ratio	$(b_3/b_2)^{max}$	10
Nozzle loss coefficient	ζ_s	0.15
Nozzle outlet blade angle	$\alpha_{b,2}$	75 deg
Rotor inlet blade angle	$\beta_{b,2}$	30 deg
Rotor outlet blade angle	$\beta_{b,3}$	−60 deg
Hub to shroud radius ratio at rotor outlet	$r_{h,3}/r_{s,3}$	0.4
Outlet shroud radius to inlet radius ratio	$r_{s,3}/r_2$	0.7
Primary heat exchanger		
Working fluid pressure loss	Δp_{PHE}	200 kPa
Thermal input	$\dot{Q}_{PHE}^{max}$	463 kW
Working fluid maximum temperature	$T_{PHE}^{out,max}$	300 °C
Pump		
Mechanical efficiency	$\eta_{mech,pump}$	0.9
Isentropic efficiency	$\eta_{s,pump}$	0.7
Recuperator		
Minimum temperature difference	ΔT_{recup}^{min}	30 °C
Pressure loss (hot side)	$\Delta p_{regen,hot}$	5 kPa
Pressure loss (cold side)	$\Delta p_{regen,cold}$	30 kPa
Condenser		
Minimum condensation temperature	T_{cond}^{min}	80 °C
Minimum temperature difference	ΔT_{cond}^{min}	20 °C
Pressure loss (hot side)	$\Delta p_{cond,hot}$	0 kPa
Pressure loss (cold side)	$\Delta p_{cond,cold}$	0.5 kPa
Fans mechanical efficiency	$\eta_{mech,fan}$	0.9025
Fans isentropic efficiency	$\eta_{s,fan}$	0.85

$$\Omega = \frac{60}{\pi} \cdot \frac{u_2}{2 \cdot r_2} \tag{23}$$

$$M_{w_2} = \frac{w_2}{c_{S,2}} \tag{24}$$

where $c_{S,2}$ is the speed of sound of the fluid, calculated by the PC-SAFT thermodynamic model.

3 Case Study: High-Temperature Organic Rankine Cycle Power Plant

The potential of the proposed 1-stage CoMT-CAMD method is demonstrated with an exemplary test case, namely, the design of a small-scale high-temperature ORC unit. This choice stems from the following considerations. First, the interrelations between working fluid selection, thermodynamic cycle design, and turbine preliminary sizing are expected to become relevant when the power capacity of the plant is small, i.e., lower than 500 kW. Second, the economic viability of ORC units of few hundred kW is arguably achievable only in the case of high conversion efficiency, which is, in turn, achievable only if the energy is available at relatively high temperature. Moreover, the application of 1-stage CoMT-CAMD to the test case at hand can lead to the identification of new promising working fluid candidates. This is a relevant achievement because the number of working fluids that are suitable for high-temperature ORC power plants is rather limited if compared to that for low-temperature systems.

The main design data specific to the adopted exemplary system are reported in Table 1, while the upper and lower bounds defined for the process design variables and the upper limit for

the number of functional groups pertaining to a candidate molecular structure are given in Table 2. The power of the thermal source has been set to achieve a power output of the ORC unit of about 100 kW. According to Ref. [1], the system under study is classifiable as a small-scale ORC turbogenerator. Furthermore, the maximum allowed temperature of the ORC is assumed as $T_{PHE}^{out,max} = 300\,°C$. This temperature level is characteristic, e.g., of biomass-fired ORC plants [10] or of small capacity units for distributed thermal solar power conversion, a concept which is currently receiving increasing attention, see, e.g., Refs. [59–61]. The main reason of this interest is due to the expectation that the economic viability for thermal solar power plants can be achieved through high-volume manufacturing of small-capacity modular systems, suitable for distributed energy conversion, rather than larger centralized power stations [62]. With respect to photovoltaic systems, the advantages are that the conversion efficiency is higher, heat cogeneration can be easily implemented, and that dispatchable electricity generation is possible with thermal storage.

A maximum cycle temperature of 300 °C might not be feasible for all the organic working fluids assessed during the solution of the optimization problem (1)–(9). The thermal decomposition temperature of the working fluids in contact with containing materials is evaluated only a posteriori and working fluids that do not feature adequate thermal stability are discarded. The value of the parameters assumed in Table 1 for the system equipment, such as the pressure drop Δp and the minimum temperature difference ΔT^{min} in the heat exchangers, or the efficiencies of the equipment constituting the pump group, follow the common practice for commercial ORC systems. Note that the pressure drop of the components forming the cold part of the ORC loop, namely, that between the turbine and the pump is assumed fixed and localized at the recuperator outlet. This is the reason why the working fluid pressure drop in the condenser is set equal to 0 kPa. The constraints and assumptions pertaining to the turbine design have to be taken as indicative since the information available in the literature about the manufacturing and operating limitations of small-scale turbo-expanders is still limited. The upper bound of the turbine inlet pressure is set equal to 30 bar or 80% of the critical pressure of the working fluid under investigation, whichever value results lower. Supercritical cycle configurations are, indeed, seldom selected in high-temperature ORC applications, while a design pressure of 30 bar for the PHE represents the technological limit for the types of heat exchangers commonly adopted in small-scale power plants. In the condenser, a direct air cooling system is considered, together with a relatively high value of the minimum condensing temperature, namely, $T_{cond}^{min} = 80\,°C$. This assumption stems from the need to contain the investment costs and footprint of the cooling system, given the small power capacity of the application. Moreover, a high condensing temperature allows for heat cogeneration. For instance, the hot air can be used for drying wood or raw materials in the food industry.

Table 2 Upper and lower bounds of the design variables of the ORC system

Parameter	Range
Mass flow rate	$0.01\,\frac{kg}{s} \leq \dot{m}_{wf} \leq 100\,\frac{kg}{s}$
Pressure at PHE outlet	$p_{out,cond} \leq p_{out,PHE} \leq 30\,bar$
Pressure at condenser outlet	$0.05\,bar \leq p_{out,cond} \leq p_{out,PHE}$
Degree of superheating	$0\,K \leq \Delta T_{sh} \leq 200\,K$
Isentropic reaction degree	$0.15 \leq R_s \leq 0.5$
Number of functional groups	$2 \leq \sum_{i \in I} y_i^S \leq 25$

Table 3   1-stage CoMT-CAMD results for the test case: the target and top ten identified working fluids as well as corresponding pure component parameters of PC-SAFT and thermodynamic cycle parameters

Rank	Component	m	σ (Å)	$\frac{\varepsilon}{k}$ (K)	MW (g mol^{-1})	T_{crit}[a] (K)	ψ[a]	P_{net} (kW)	η_{th} (%)	p_1 (MPa)	ΔT_{sh} (K)	T_1 (K)
—	Target	1.68	4.80	364.6	117.8	602.7	18.7	103.3	22.3	2.46	11	573
1	Methyl-cyclohexane	2.62	4.03	286.4	98.2	586.3	10.2	101.3	21.9	2.17	36	573
2	Cyclohexane	2.37	3.91	289.0	84.2	565.2	6.4	101.0	21.8	3.00	43	573
3	Dimethyl-cyclopentane	2.69	3.95	275.6	98.2	571.6	10.0	100.4	21.7	2.68	33	573
4	2,2,3,3-tetramethyl-butane	2.33	4.39	300.1	114.2	582.4	16.7	99.9	21.6	2.32	24	573
5	Toluene	2.88	3.74	278.4	92.1	595.3	6.1	99.6	21.5	1.83	48	573
6	Ethyl-cyclopentane	2.97	3.86	266.7	98.2	577.7	9.8	99.4	21.5	2.13	42	573
7	Trimethyl-cyclopentane	2.87	4.04	279.0	112.2	595.4	14.4	98.4	21.3	1.53	45	573
8	3,4,4-trimethyl-1-pentene[b]	2.85	4.09	269.6	112.2	573.9	14.1	98.2	21.2	2.13	35	573
9	Dimethyl-cyclohexane	2.86	4.11	284.2	112.2	605.7	14.4	98.1	21.2	1.24	48	573
10	Benzene	2.54	3.73	274.4	78.1	554.2	2.4	97.7	21.1	3.00	57	573
Benchmark solutions												
—	Cyclopentane	2.34	3.73	267.2	70.1	519.1	2.6	88.7	19.2	3.00	92	573
—	MM[c]	4.12	4.02	212.5	162.4	525.4	15.1	89.0	19.2	1.73	62	573
—	MDM[c]	5.33	4.12	209.6	236.5	567.2	27.9	80.2	17.3	0.56	69	573

Note: As benchmark, solutions with fluids commonly adopted in high-temperature ORC applications are reported, namely, Cyclopentane, MM (hexamethyldisiloxane), and MDM (octamethyltrisiloxane).
[a]According to the adopted EoS model, see Sec. 2.1.
[b]3,3,4-trimethyl-1-pentene. The adopted method does not distinguish among isomers.
[c]The PC-SAFT pure component parameters are directly fitted to measurement data. The dipole moment of MM and MDM is $\mu = 0.66$ D and $\mu = 1.08$ D, respectively, while for all the other identified fluids, the dipole moment is $\mu = 0$ D.

Regarding the turbine preliminary design, the values of the design variables are fixed, see Table 1, except for the isentropic reaction degree R_s. Their definition is based on design recommendations and preliminary exploration of the radial-inflow turbine design space. As an example, optimal values reported in the literature for $r_{s,3}/r_2$ are in the range of 0.4–0.7 [63]. The outlet shroud radius to inlet radius ratio is set here to $r_{s,3}/r_2 = 0.7$ in order to attain higher blade heights at the rotor inlet, thereby maximizing the efficiency and the feasible design space of the turbine. This, in turn, allows for larger turbine pressure ratios, which are usually beneficial for the conversion efficiency of the thermodynamic cycle. Similar considerations have been made for the other geometric quantities. Notably, the hub to shroud radius ratio at the rotor outlet, $r_{h,3}/r_{s,3}$, is taken equal to 0.4, while the blade angles $\alpha_{b,2}$ and $\beta_{b,3}$ are 75 deg and −60 deg, respectively. The turbine adopts also a back-swept rotor configuration, see Fig. 2. The optimal range reported in the literature for $\beta_{b,2}$ is between 20 deg and 40 deg [64]. A value of 30 deg is here assumed, since larger $\beta_{b,2}$ may complicate the structural design of the impeller [65]. Conversely, a value of R_s suitable for all possible operating conditions cannot be univocally defined. For this reason, the turbine degree of reaction R_s is included among the optimization variables in Eq. (8). Thereby, the design method has also a degree-of-freedom to meet the turbine constraints in Eq. (16) and to maximize the isentropic efficiency of the expander.

Common working fluids adopted for high-temperature ORC systems belong to the family of siloxanes, alkanes, cyclic-alkanes, and aromatic hydrocarbons, see, e.g., Refs. [1,9,10], and [47]. A special mention is also deserved for perfluorocarbons, which exhibit remarkable thermal stability and have been successfully investigated in the 1980s for small-scale ORC turbogenerators [66] but are affected by a high value of the Global Warming Potential. The organic working fluids that appear more suitable for the selected temperature levels based on the literature results in Refs. [47] and [67] are toluene, cyclohexane, cyclopentane, and the linear siloxanes MM and MDM. These fluids are here considered to generate benchmark solutions for 1-stage CoMT-CAMD.

The selected objective function in Eq. (1) is the ORC net power output P_{net}, which for the case study reads

$$\max_{x, y^s} P_{\mathrm{net}} = P_{\mathrm{turbogenerator}} - P_{\mathrm{pump}} - P_{\mathrm{fan}} \qquad (25)$$

where $P_{\mathrm{turbogenerator}}$ denotes the power output of the turbogenerator, P_{pump} the power input of the pump, and P_{fan} the power input of the air condenser fans.

3.1   Results. The solution of 1-stage CoMT-CAMD leads to the identification of the organic working fluids given in Table 3. Initially, the relaxation problem is solved. The result is a hypothetical working fluid featuring a nonphysical molecular structure, named *target*, which allows for the maximum achievable net power output, i.e., $P_{\mathrm{net}} = 103.3$ kW. Subsequently, the top ten organic working fluids are identified using integer cuts. With reference to Table 3, the identified working fluids are mainly cyclopentane and cyclohexane derivatives with alkyl side chains. Besides them, the aromatic hydrocarbon benzene and its alkyl derivative toluene, the branched alkane tetramethyl-butane, and the branched alkene trimethyl-pentene are found. The working fluid allowing for the maximum net power output is methyl-cyclohexane with $P_{\mathrm{net}} = 101.3$ kW, which is only 1.9% lower than the performance of the target. A common feature of the optimal solutions is that the maximum cycle temperature is always equal to the upper limit selected for T_1, see Table 1. Analogous consideration applies to the condensing temperature, whose optimal value corresponds to the lower limit $T_{\mathrm{cond}}^{\mathrm{min}}$ set in the optimization for T_6. All working fluids also exhibit a similar critical temperature, in the range between 570 K and 600 K. On the other hand, their molecular complexity differs quite significantly. A quantity that well represents the molecular complexity is the coefficient ψ defined as

$$\psi \equiv \frac{T_{\mathrm{crit}}}{R} \left(\frac{\partial s_{sv}}{\partial T} \right) \bigg|_{T_r = 0.7} \qquad (26)$$

where s_{sv} is the saturated-vapor entropy calculated at a reduced temperature of 0.7 [68]. ψ is commonly referred to as the molecular complexity parameter and is proportional to the heat capacity of the saturated vapor and, thus, is directly related to the molecular structure of the fluid [69]. Together with the critical temperature, ψ is found to most influence the cycle performance and its optimal configuration. Notably, the slope of the dew line in the temperature–entropy (T–s) diagram is positive if $\psi \geq 0$ and tends to become steeper as the value of ψ increases [69]. As a consequence, the higher the molecular complexity of the working fluid,

Table 4 Results of turbine preliminary design for the working fluids listed in Table 3

| Rank	Component	η_S (%)	R_s	b_2 (mm)	ω (rpm)	$M_{w,2}$	$\dfrac{b_3}{b_2}$	$\dfrac{p_1}{p_4}$
—	Target	85.8	0.46	3.1	42,860	0.47	10.0	38.6
1	Methyl-cyclohexane	85.4	0.47	3.0	48,270	0.46	10.0	38.7
2	Cyclohexane	86.4	0.44	2.5	60,394	0.46	10.0	28.6
3	Dimethyl-cyclopentane	85.7	0.47	2.7	52,141	0.46	10.0	37.9
4	2,2,3,3-tetramethyl-butane	85.7	0.47	3.1	43,591	0.47	10.0	38.9
5	Toluene	85.4	0.48	3.1	48,089	0.46	10.0	38.3
6	Ethyl-cyclopentane	85.4	0.47	3.0	48,377	0.46	10.0	38.6
7	Trimethyl-cyclopentane	85.2	0.48	3.5	38,652	0.46	10.0	39.0
8	3,4,4-trimethyl-1-pentene	85.5	0.47	3.1	43,318	0.47	10.0	39.0
9	Dymethyl-cyclohexane	85.2	0.48	3.8	35,398	0.46	10.0	38.9
10	Benzene	86.5	0.43	2.4	65,056	0.44	9.6	23.9
Benchmark solutions								
—	Cyclopentane	85.7	0.41	2.4	70,000	0.40	9.0	11.6
—	MM	86.7	0.43	3.7	29,998	0.47	10.0	29.5
—	MDM	85.3	0.48	6.3	15,111	0.47	10.0	39.5

the greater the degree of regeneration. The resulting impact on conversion efficiency is generally positive. Angelino et al. [68] investigated the trend of thermodynamic cycle performance versus the molecular complexity of the working fluid. They demonstrated that for the recuperated cycle configuration commonly adopted in high-temperature ORC systems, η_{th} increases with increasing values of ψ, till a maximum is reached. Subsequently, the correlation between these two parameters becomes weak and a plateau in η_{th} is observed. Angelino et al. [68] also found that the range of ψ corresponding to the maximum conversion efficiency depends on the upper and lower temperature level of the cycle. According to their results, the optimal working fluids for the studied application should feature a molecular complexity between 15 and 20. This trend is reflected in the data in Table 3 only to a minor extent. ψ of the top ten candidates identified by the 1-stage CoMT-CAMD method varies from 2.4 of benzene to 16.7 of tetramethyl-butane. Despite the quite different molecular complexity, their performance does not significantly differ: the estimated ORC net power output varies between $P_{net} = 98$ kW and $P_{net} = 101$ kW, namely, within the expected uncertainty range of the model [22]. The reason for the mismatch between these results and those of Ref. [68] can be explained by analyzing the result of the turbine preliminary sizing reported in Table 4. Notably, although the turbine geometries vary with the working fluid, there is one design constraint affecting almost all the optimum solutions identified by the method: the outlet to inlet blade height ratio b_3/b_2 of the impeller, whose upper bound has been set equal to ten. Its effect is a limitation on the overall expansion ratio of the turbine and consequently, on the maximum cycle pressure, which leads to high degrees of superheating of the vapor at the turbine inlet, see Table 3. Hence, the ultimate result is a reduction in the net power output achievable by using organic working fluids of increasing molecular complexity.

On the other hand, if system design is repeated without considering the constraint on the b_3/b_2 ratio, the best working fluids found by the 1-stage CoMT-CAMD method exhibit values of ψ that are more uniform and closer to the optimal range indicated by Angelino et al. [68]. In particular, xylene ($T_{crit} = 631.8$ K, $\psi = 10.4$) becomes the best working fluid, followed by ethyl-cyclohexane ($T_{crit} = 614.0$ K, $\psi = 14.5$) with a net power output of 106 kW and 105.3 kW, respectively. Dimethyl-cyclohexane is ranked third with $P_{net} = 104.8$ kW, while it is only the ninth option if the constraint on the b_3/b_2 ratio is activated, see Table 3. All three solutions feature an infeasible turbine geometry. This result shows the importance of integrating the design of the thermodynamic cycle and working fluid with the preliminary sizing of the turbine in order to correctly identify the optimal working fluids for a small-scale ORC system.

The value of the isentropic turbine efficiency η_s estimated for the fluid candidates identified by the method is in the range between 85% and 87%, see Table 4. Such a relatively small difference in performance can be explained by the rather similar turbine geometry obtained for the optimal working fluids. This result is mainly a consequence of the fact that the geometric ratios $r_{h,3}/r_{s,3}$ and $r_{s,3}/r_2$ have been taken as constant in the design procedure. In addition, the turbine efficiency is arguably the model parameter affected by the largest uncertainty, since the adopted fluid-dynamic loss correlations were calibrated for gas/air radial-inflow machines. Their accuracy has never been assessed for ORC applications, which are characterized by much higher pressure and volumetric flow ratios. For all identified working fluids, the fluid kinetic energy at the impeller outlet is equivalent to approximately 3.2–4.5% points of the turbine efficiency. Thus, the gain in performance achievable with a diffuser will be relatively low, and an economic analysis would be required to justify the use of a diffuser.

Regarding the benchmark solutions, toluene and cyclohexane are ranked among the optimal working fluids, while cyclopentane, MM, and MDM provide a significantly lower estimated performance. This is mainly due to the high degree of superheating needed to meet the turbine preliminary design constraints, and, in the case of cyclopentane, also to the constraint on the maximum cycle pressure, here limited to 30 bar or 80% of the critical pressure. The effect is a reduction in the average temperature at which thermal energy is transferred into the system, which consequently penalizes its conversion efficiency.

3.2 A Posteriori Evaluation of the Working Fluids. The selection of the working fluid for an actual application cannot be performed independently from an analysis of the melting point, toxicity, thermal stability, and flammability of the identified candidates. Almost all identified working fluids show a melting point that is lower than 10 °C with the exception of 2,2,3,3-tetramethyl-butane, which solidifies at about 100 °C due to its highly branched and compact structure. 2,2,3,3-tetramethyl-butane is thus not suitable as working fluid. With respect to toxicological properties, cyclic alkanes are generally classified as less harmful than aromatic hydrocarbons and thus they are preferable. However, they exhibit lower thermal stability. For instance, cyclopentane, which is the sole cyclic alkane whose thermal resistance has been thoroughly tested, is thermally stable up to 300–350 °C [70,71] versus a maximum operating temperature of benzene and toluene of about 350–400 °C [68,72]. Cyclohexane is expected to feature thermal stability similar to the thermal stability of cyclopentane given the analogous molecular structure, although no
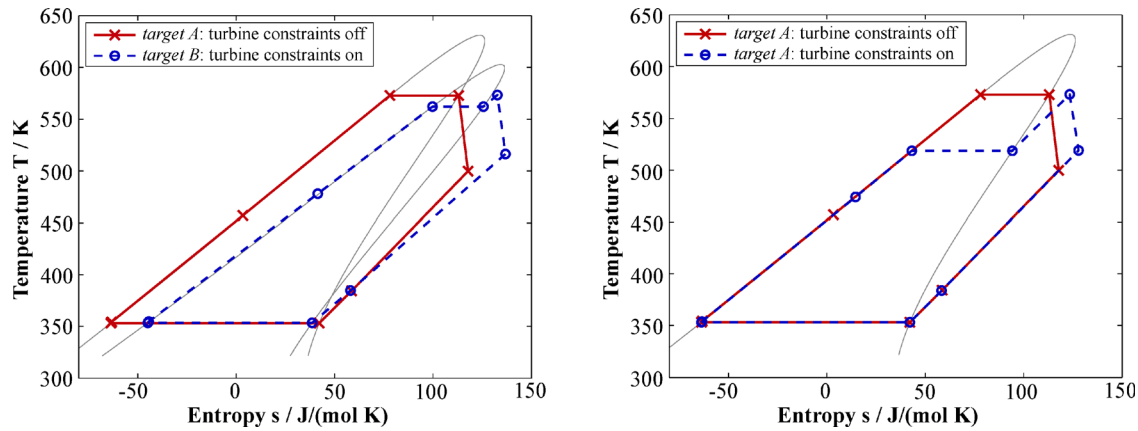
Fig. 4 Effect of constraints concerning turbine preliminary design on optimal thermodynamic cycle configuration and working fluid: (left) temperature–entropy diagram of the target in the case the turbine design constraints are neglected during optimization (target A, ——, $P_{net} = 107.1$ kW) or considered (target B, - - -, $P_{net} = 103.3$ kW) and (right) temperature–entropy diagram of target A when turbine constraints are neglected during optimization (——) or considered (- - -, $P_{net} = 96.8$ kW)

experimental tests have been published to date [47]. Regarding the thermal decomposition of the alkyl-derivatives of cyclopentane and cyclohexane in Table 3, no data have been found in the literature for the temperature levels of interest in ORC applications. On the one hand, thermal stability tends to decrease with branched working fluids. Thus, the more side chains exist in the molecular structure, the more the allowed maximum temperature of the working fluid is expected to decrease with respect to the maximum temperature achievable by the equivalent fluid forming the backbone of the molecule. On the other hand, Angelino et al. [68] investigated experimentally the decomposition of some methyl-substituted benzenes at temperature levels around 400 °C, which is considered the upper operating limit for benzene; the authors discovered that toluene and trimethylbenzene seemingly have the same thermal stability and they can be safely employed in ORC engines with top temperatures up to 380 °C. Due to these considerations, the identified methyl-substituted cyclopentanes and cyclohexanes might exhibit a thermal stability close to the thermal stability of cyclopentane, i.e., up to 300 °C. Such a thermal stability would make the identified methyl-substituted cyclopentanes and cyclohexanes, together with cyclohexane, promising working fluid candidates for high-temperature small capacity ORC systems. Nevertheless, experimental tests as those described in Refs. [72] and [73] are required before such organic working fluids can be actually used at the temperature levels assumed here. The adoption of methyl-substituted cycloalkanes as working fluid in high-temperature ORC systems, to the best of the authors' knowledge, has been considered only in Ref. [55]. The work documents the successful testing of an ORC turbogenerator that operates with methylcyclohexane at a maximum cycle temperature around 245 °C. The net power of the prototype is about 70 kW. The results of the study supply a confirmation, although partial, of the thermal stability of such a fluids class and its suitability for small-scale ORC units.

Concerning the molecules ranked as numbers 6 and 8 in Table 3, their thermal stability is also unknown. However, this is expected to be lower than the thermal stability of methyl-substituted cycloalkanes, because either the molecule forming the backbone chain is less stable than cyclopentane/cyclohexane, as, in the case of trimethyl-1-pentene and related isomers, or the side chain is more prone to decomposition than the methyl group, as for ethyl-cyclopentane. The ethyl group, indeed, features bond energy lower than that associated with the methyl group.

Besides toxicity and thermal stability, a major factor driving working fluid selection is flammability. In this work, flammability is assessed based on the H200 codes of the globally harmonized

system for classification and labeling of chemicals (GHS), which indicate the hazards associated with a chemical substance, including the risk of explosion and flammability [74]. The identified working fluids feature the same classification as the benchmark fluids cyclopentane and MM. Since these two benchmark fluids are largely adopted in high-temperature ORC applications, safe operation with the other working fluids in Table 3 is assumed to be possible.

Finally, note that toluene and cyclohexane are ranked among the top ten working fluids. This may suggest that there is no benefit in adopting the proposed method in place of the traditional design approach, provided that the preliminary sizing of the turbine is integrated into the design of the thermodynamic cycle. However, in the authors' opinion, the solution to the exemplary test case considered here reveals several advantages. By means of the 1-stage CoMT-CAMD method, it is possible to (i) methodically assess a large set of working fluid candidates in a short computational time (i.e., 1 h to 10 h are required to calculate a ranking of ten working fluids using an Intel-Xeon CPU with 3.0 GHz and 64 GB RAM depending on the set of functional groups and considered constraints), (ii) gain a clearer understanding of which thermodynamic characteristics the working fluid should exhibit, and (iii) possibly spot new working fluid families. The fact that methyl-substituted cycloalkanes have been so far overlooked as working fluid for high-temperature small-capacity ORC power plants arguably confirms the potential of the proposed method.

3.3 Influence of Turbine Preliminary Design Constraints on Fluid Selection. The 1-stage CoMT-CAMD method can also be used to understand and assess the relationships between fluid properties, thermodynamic cycle parameters, and turbine geometry for the specific ORC application under investigation. Evidence of the strong interdependence existing among these variables in small-scale ORC systems is provided by Fig. 4(a), which shows, for the test case of Sec. 3.1, how the characteristics of the optimal thermodynamic cycle depend on considering the constraints associated with the turbine preliminary design.

The working fluids underlying the thermodynamic cycles are not real fluids but the hypothetical fluids that result from relaxing the original optimization problem. As already mentioned, the solution to the relaxation problem is a molecule, called target, which allows for the maximum power output. However, it features a nonphysical molecular structure. With reference to Fig. 4(a), target A is the solution to the relaxation problem when the turbine design constraints are neglected, while target B refers to the test case where the turbine design constraints are considered.

Table 5 1-stage CoMT-CAMD results for the test case at hand when $\Omega^{max} = 24{,}000$ rpm: the target and top five identified working fluids as well as corresponding PC-SAFT pure component parameters and main thermodynamic cycle parameters

Rank	Component	m	σ (Å)	$\frac{\varepsilon}{k}$ (K)	MW (g mol^{-1})	T_{crit}[a] (K)	ψ[a]	P_{net} (kW)	η_{th} (%)	p_1 (MPa)	ΔT_{sh} (K)	T_1 (K)
—	Target	1.99	4.87	365.0	143.3	656.8	29.3	96.7	20.9	0.77	43	573
1	Trimethyl-cyclohexane	3.11	4.19	282.4	126.2	623.7	19.0	91.6	19.8	0.61	69	573
2	3,3,4,4-tetramethyl-1-hexen[b]	3.11	4.27	288.6	140.3	637.5	25.0	90.5	19.5	0.59	58	573
3	2,2,3,3,4-pentamethylpentane[c]	3.09	4.30	288.4	142.3	635.2	26.5	90.4	19.5	0.61	57	573
4	2-ethoxy-2,3,3-trimethyl-butane[d,e]	3.47	4.07	263.1	144.3	612.5	22.4	90.3	19.5	0.72	61	573
5	Tertmethyl Cyclopentane	3.05	4.11	282.1	126.2	617.8	19.2	89.6	19.4	0.62	78	573
Benchmark solutions												
—	MM	4.12	4.02	212.5	162.4	525.4	15.1	80.6	17.4	1.02	91	569
—	Toluene	2.88	3.74	278.4	92.1	595.3	6.1	68.5	14.8	0.46	100	543
—	Cyclohexane	2.37	3.91	289.0	84.2	565.2	6.4	52.0	11.2	0.55	74	497
—	Cyclopentane	2.34	3.73	267.2	70.1	519.0	2.6	33.0	7.1	0.73	65	463

Note: As benchmark, the same information is reported for thermodynamic cycles adopting as working fluid MM (hexamethyldisiloxane), toluene, cyclohexane, and cyclopentane.
[a]According to the adopted EoS model, see Sec. 2.1.
[b]Equivalent isomers 3,3,5,5-tetramethyl-1-hexen and 4,4,5,5-tetramethyl-1-hexen.
[c]Equivalent isomer 2,2,3,4,4-pentamethylpentane.
[d]Equivalent isomer 1-tert-butoxy-2,2-dimethyl-propane.
[e]The PC-SAFT pure component parameters for these fluids include also a dipole moment of $\mu = 2.7$ D.

Table 6 Results of turbine preliminary design for the working fluids listed in Table 5

Rank	Component	η_S (%)	R_s	b_2 (mm)	ω (rpm)	$M_{w,2}$	$\frac{b_3}{b_2}$	$\frac{p_1}{p_4}$
—	Target	86.0	0.47	5.1	24,000	0.47	10.0	36.4
1	Trimethyl cyclohexane	86.8	0.45	5.4	24,000	0.46	10.0	31.5
2	3,3,4,4-tetramethyl-1-hexen	85.1	0.49	5.5	22,439	0.46	10.0	38.7
3	2,2,3,3,4-pentamethylpentane	85.1	0.49	5.4	22,545	0.46	10.0	38.7
4	2-ethoxy-2,3,3-trimethyl-butane	85.2	0.48	5.1	24,000	0.46	10.0	38.6
5	Tertmethyl cyclopentane	87.1	0.43	5.4	24,000	0.46	10.0	26.9
Benchmark solutions								
—	MM	86.6	0.41	4.5	24,000	0.44	10.0	17.4
—	Toluene	85.9	0.39	5.3	24,000	0.39	10.0	9.5
—	Cyclopentane	84.5	0.38	4.6	24,000	0.34	10.0	5.2
—	Cyclopentane	83.1	0.38	3.8	24,000	0.27	10.0	2.8

As well known in the literature [68,75], the optimum ORC configuration, from an efficiency point of view, is a saturated cycle where the evaporation occurs at T_{max}, as for the thermodynamic cycle for target A in Fig. 4(a). However, this solution features a turbine volumetric flow ratio which is too high, leading to an excessive value of the inlet to outlet blade height ratio of the impeller ($b_3/b_2 = 15.9$). To meet the turbine design requirements with target A as working fluid, the pressure ratio of the cycle must be lower, see Fig. 4(b), thus resulting into a high degree of superheating of the vapor at the turbine inlet. The net power output of the ORC system is approximately 10% lower. It reduces from 107.1 kW to 96.8 kW. In contrast, if turbine design constraints are considered while performing the integrated fluid selection and cycle design calculation, the optimizer identifies a different hypothetical molecule, i.e., target B in Fig. 4(a), which is characterized by a higher molecular complexity than target A, as evident from the greater slope of the dew line in the temperature–entropy (T–s) thermodynamic diagram. The key advantage of the new target is the lower boiling point, although this comes at the cost of a decrease in the critical temperature of the fluid. The effect is a reduction of the volumetric flow rate and the pressure ratio across the expander. Thus, the fulfillment of the design constraints requires a minimum degree of superheating at the PHE outlet. Due to the limitations associated with the turbine preliminary design, the penalty on the net power output is lower than for target A, being for target B $P_{net} = 103.3$ kW.

A large degree of superheating is mandatory if tighter constraints on the maximum rotational speed of the turbine Ω^{max} and the minimum blade height at the rotor inlet b_2^{min} are chosen. To demonstrate the impact of a tighter constraint on Ω^{max}, the analysis of the case study of Sec. 3 is repeated with $\Omega^{max} = 24{,}000$ rpm. This value is representative of the speed of several ORC turbogenerators currently on the market [76,77]. The results of the design exercise are summarized in Table 5 and Table 6, which, respectively, report (i) the thermodynamic characteristics and main cycle parameters for the target and the top five working fluids identified by the 1-stage CoMT-CAMD method, and (ii) the results of the turbine preliminary design for the same working fluids. For comparison, the tables list also the data for the benchmark working fluids toluene, cyclopentane, cyclohexane, and MM. The data for MDM are not reported because these results remain identical to those reported in Tables 3 and 4. It is apparent that the molecular complexity of the optimal candidates is now much higher than in the previous case study. The degree of superheating ΔT_{sh} is significantly larger such that the volumetric flow rate across the turbine is larger, thus meeting the requirements on the inlet to outlet blade height ratio of the impeller b_3/b_2 as well as on the maximum rotational speed of the turbine Ω^{max}. Here, the limitation on the maximum rotational speed is an active constraint for most of the solutions in Table 5.

The rationale behind these optimization results can be explained by recalling that an increase in the molecular

complexity ψ leads, in general, to a higher volumetric flow rate and pressure ratio across the expander, as a consequence of the higher boiling point of the fluid. At the same time, the enthalpy difference over the expansion remains almost constant [69], at least for the typical levels of molecular complexity of the working fluids of interest in ORC applications. The positive effect is a reduction in the rotational speed of the turbine along with an increment of the blade height at the rotor inlet b_2. On the other hand, the ratio b_3/b_2 and the relative Mach number at the rotor inlet $M_{w,2}$ tend to increase. Due to these counteracting effects, the optimizer satisfies the chosen design requirements by both increasing the molecular complexity of the working fluid and reducing the cycle pressure ratio. Moreover, the degree of regeneration in the cycle augments with a rise in the molecular complexity ψ of the working fluid. This partially compensates for the negative impact on thermodynamic efficiency of a large degree of superheating, which tends to reduce the average temperature at which thermal energy is transferred to the cycle.

The adoption of a working fluid featuring a simple molecular structure would always lead to suboptimal cycle performance, as demonstrated by the very low power output obtained in case cyclopentane is the working fluid. If the turbine inlet temperature T_1 is taken equal to $T_{PHE}^{out,max}$ as for the more molecularly complex fluids, the degree of superheating needed to satisfy the turbine design constraints would be excessively high. The resulting penalty on system efficiency proves to be more detrimental than reducing the maximum cycle temperature. This explains why the value calculated by the optimizer for T_1 tends to decrease as the molecular complexity of the working fluids used to generate the benchmark solutions reduces. Conversely, the optimal value for the minimum cycle temperature always remains at its lower bound, i.e., 353 K.

4 Conclusions

The 1-stage CoMT-CAMD method was recently conceived by some of the authors as a preliminary ORC power plant design procedure, integrating the selection of the working fluid and the optimization of the thermodynamic cycle into a single optimization process. In this work, the integrated design method has been complemented with a meanline design model of a radial-inflow turbine to bound the search space of the optimization problem to regions where the design of the turbine is feasible. The isentropic efficiency of the turbine is calculated during the optimization depending on the process parameters and the adopted working fluid. The constraints on the turbine design reduce the feasible design space of the ORC system, depending on the working fluid characteristics and power capacity of the application. The resulting method has been tested considering a high-temperature small-scale ORC unit adopting a radial-inflow turbo-expander as case study. The analysis of the results for this exercise led to the following conclusions:

- The key advantage of the proposed design method over the commonly used sequential design practice is the capability to identify the optimal working fluids given the constraints of the application under investigation, including those related to the system equipment. This significantly reduces the time needed to accomplish the whole design process, especially in the case of mini- or small-scale ORC systems, since it avoids the iterative computations required for each working fluid candidate to define a feasible combination of thermodynamic cycle parameters and turbine design specifications. Moreover, such a combination is usually the result of a trial and error approach, which might often lead to suboptimal results due to the large number of design variables and constraints, and the complex interrelations among them.
- The method allows considering a large set of feasible molecular structures. This is particularly helpful in the case of novel applications, since the optimal working fluids may belong to fluid classes, which might be overlooked in the traditional design practice. Theoretically, it is also possible that the optimal molecular structure does not correspond to a working fluid existing in common databases: the result of the method might thus initiate the study and possibly synthesis of new chemicals.
- In the case of small-scale ORC systems, the study confirms that the turbine design constraints considerably influence the choice of the optimal working fluid and the corresponding thermodynamic cycle parameters. Notably, the more stringent the constraints on the rotational speed of the turbine Ω and the blade height at the rotor inlet b_2, the more molecularly complex is the optimal working fluid. The reason is that the degree of regeneration of the cycle tends to increase with larger molecular complexity. This partially compensates for the negative impact on thermodynamic efficiency of the large degree of superheating needed to meet the limitations related to the turbine preliminary design.
- Methyl-substituted cycloalkanes are promising fluid candidates for high-temperature small capacity ORC systems. However, extensive thermal stability tests are required before such organic working fluids can be actually used at the temperature levels considered in this study.

The presented 1-stage CoMT-CAMD method enables a holistic design of the optimal working fluid and the corresponding optimal thermodynamic cycle and turbine. The proposed method is generally applicable to the design of any ORC process, whatever turbine configuration is chosen. The application of the method to larger power output units will simply require an adaptation of the meanline code to include other common turbine configurations, namely, axial and radial outflow [1]. Future work will be devoted to include the preliminary design of heat exchangers into the procedure such that a thermo-economic optimization of the ORC plant may be performed as described in Refs. [23] and [30].

Nomenclature

Symbols

b = blade height
c = absolute velocity
c_P = specific heat at constant pressure
c_S = speed of sound
f = objective function
F_1/F_2 = CAMD constraints
g_1/g_2 = system model constraints
h = enthalpy
k = Boltzmann constant
m = number of segments per chain
$\dot{m}$ = mass flow rate

M = Mach number
MW = molecular weight
p = pressure
P = mechanical/electric power
$\dot{Q}$ = thermal power
r = radius
R = reaction degree, gas constant
s = entropy
T = temperature
u = peripheral speed
w = relative velocity
x = process variables
y^S = molecular structure
z = pure component parameters

Greek Symbols

α = nozzle flow angle
α_b = nozzle blade angle
β = rotor flow angle
β_b = rotor blade angle
Δ = difference
ε = depth of pair potential
$\varepsilon^{A,B}$ = associating energy
ζ = loss coefficient
η = efficiency
θ = thermodynamic properties
$\kappa^{A,B}$ = associating volume
μ = dipole moment
ρ = density
σ = segment diameter
ψ = load coefficient
Ω = rotational speed

Subscripts

cond = condenser
crit = critical
gen = electric generator
h = hub
mech = mechanical
n = nozzle
PHE = primary heat exchanger
r = rotor, reduced propriety
regen = regenerator
s = isentropic, shroud
sh = superheating
ss = stage isentropic
sv = saturated-vapor
wf = working fluid
0 = total conditions
1 = nozzle/stator inlet
2 = nozzle/stator outlet
3 = rotor outlet
4 = diffuser outlet

Superscript

ig = ideal gas

Abbreviations

CAMD = computer-aided molecular design
CoMT = continuous-molecular targeting
DICOPT = discrete and continuous optimizer
EoS = equation of state
GAMS = general algebraic modeling system
MDM = octamethyltrisiloxane
MINLP = mixed-integer nonlinear programming
MM = hexamethyldisiloxane
ORC = organic Rankine cycle

PC-SAFT = perturbed-chain statistical associating fluid theory
PHE = primary heat exchanger
RIT = radial-inflow turbine
SAFT = statistical associating fluid theory

References

[1] Colonna, P., Casati, E., Trapp, C., Mathijssen, T., Larjola, J., Turunen-Saaresti, T., and Uusitalo, A., 2015, "Organic Rankine Cycle Power Systems: Rom the Concept to Current Technology, Applications, and an Outlook to the Future," ASME J. Eng. Gas Turbines Power, **137**(10), p. 100801.
[2] Tchanche, B. F., Papadakis, G., Lambrinos, G., and Frangoudakis, A., 2009, "Fluid Selection for a Low-Temperature Solar Organic Rankine Cycle," Appl. Therm. Eng., **29**(11–12), pp. 2468–2476.
[3] Heberle, F., and Brüggemann, D., 2010, "Exergy Based Fluid Selection for a Geothermal Organic Rankine Cycle for Combined Heat and Power Generation," Appl. Therm. Eng., **30**(11–12), pp. 1326–1332.
[4] Quoilin, S., Declaye, S., Tchanche, B. F., and Lemort, V., 2011, "Thermo-Economic Optimization of Waste Heat Recovery Organic Rankine Cycles," Appl. Therm. Eng., **31**(14–15), pp. 2885–2893.
[5] Lang, W., Colonna, P., and Almbauer, R., 2013, "Assessment of Waste Heat Recovery From a Heavy-Duty Truck Engine by Means of an ORC Turbogenerator," ASME J. Eng. Gas Turbines Power, **135**(4), p. 042313.
[6] Quoilin, S., van Broek, M. D., Declaye, S., Dewallef, P., and Lemort, V., 2013, "Techno-Economic Survey of Organic Rankine Cycle (ORC) Systems," Renewable Sustainable Energy Rev., **22**, pp. 168–186.
[7] Bao, J., and Zhao, L., 2013, "A Review of Working Fluid and Expander Selections for Organic Rankine Cycle," Renewable Sustainable Energy Rev., **24**, pp. 325–342.
[8] Linke, P., Papadopoulos, A., and Seferlis, P., 2015, "Systematic Methods for Working Fluid Selection and the Design, Integration and Control of Organic Rankine Cycles—A Review," Energies, **8**(6), pp. 4755–4801.
[9] Lai, N. A., Wendland, M., and Fischer, J., 2011, "Working Fluids for High-Temperature Organic Rankine Cycles," Energy, **36**(1), pp. 199–211.
[10] Drescher, U., and Brüggemann, D., 2007, "Fluid Selection for the Organic Rankine Cycle (ORC) in Biomass Power and Heat Plants," Appl. Therm. Eng., **27**(1), pp. 223–228.
[11] Maizza, V., and Maizza, A., 2001, "Unconventional Working Fluids in Organic Rankine-Cycles for Waste Energy Recovery Systems," Appl. Therm. Eng., **21**(3), pp. 381–390.
[12] Wang, Z. Q., Zhou, N. J., Guo, J., and Wang, X. Y., 2012, "Fluid Selection and Parametric Optimization of Organic Rankine Cycle Using Low Temperature Waste Heat," Energy, **40**(1), pp. 107–115.
[13] Schwöbel, J. A. H., Preißinger, M., Brüggemann, D., and Klamt, A., 2017, "High-Throughput Screening of Working Fluids for the Organic Rankine Cycle (ORC) Based on Conductor-Like Screening Model for Realistic Solvation (COSMO-RS) and Thermodynamic Process Simulations," Ind. Eng. Chem. Res., **56**(3), pp. 788–798.
[14] Preißinger, M., Schwöbel, J. A., Klamt, A., and Brüggemann, D., 2017, "Multi-Criteria Evaluation of Several Million Working Fluids for Waste Heat Recovery by Means of Organic Rankine Cycle in Passenger Cars and Heavy-Duty Trucks," Appl. Energy, **206**, pp. 887–899.
[15] Papadopoulos, A. I., Tsivintzelis, I., Linke, P., and Seferlis, P., 2018, "Computer-Aided Molecular Design: Fundamentals, Methods, and Applications," In: Reedijk, J. (Ed.) Elsevier Reference Module in Chemistry, Molecular Sciences and Chemical Engineering, Elsevier, Waltham, MA.
[16] Papadopoulos, A. I., Stijepovic, M., and Linke, P., 2010, "On the Systematic Design and Selection of Optimal Working Fluids for Organic Rankine Cycles," Appl. Therm. Eng., **30**(6–7), pp. 760–769.
[17] Bardow, A., Steur, K., and Gross, J., 2010, "Continuous-Molecular Targeting for Integrated Solvent and Process Design," Ind. Eng. Chem. Res., **49**(6), pp. 2834–2840.
[18] Lampe, M., Stavrou, M., Bücker, H. M., Gross, J., and Bardow, A., 2014, "Simultaneous Optimization of Working Fluid and Process for Organic Rankine Cycles Using PC-SAFT," Ind. Eng. Chem. Res., **53**(21), pp. 8821–8830.
[19] Gross, J., and Sadowski, G., 2001, "Perturbed-Chain SAFT: An Equation of State Based on a Perturbation Theory for Chain Molecules," Ind. Eng. Chem. Res., **40**(4), pp. 1244–1260.
[20] Sauer, E., Stavrou, M., and Gross, J., 2014, "Comparison Between a Homo- and a Heterosegmented Group Contribution Approach Based on the Perturbed-Chain Polar Statistical Associating Fluid Theory Equation of State," Ind. Eng. Chem. Res., **53**(38), pp. 14854–14864.
[21] Lampe, M., Stavrou, M., Schilling, J., Sauer, E., Gross, J., and Bardow, A., 2015, "Computer-Aided Molecular Design in the Continuous-Molecular Targeting Framework Using Group-Contribution PC-SAFT," Comput. Chem. Eng., **81**, pp. 278–287.
[22] Schilling, J., Lampe, M., Gross, J., and Bardow, A., 2017, "1-Stage CoMT-CAMD: An Approach for Integrated Design of ORC Process and Working Fluid Using PC-SAFT," Chem. Eng. Sci., **159**, pp. 217–230.
[23] Schilling, J., Tillmanns, D., Lampe, M., Hopp, M., Gross, J., and Bardow, A., 2017, "From Molecules to Dollars: Integrating Molecular Design Into Thermo-Economic Process Design Using Consistent Thermodynamic Modeling," Mol. Syst. Des. Eng., **2**(3), pp. 301–320.
[24] Lötgering-Lin, O., and Gross, J., 2015, "Group Contribution Method for Viscosities Based on Entropy Scaling Using the Perturbed-Chain Polar Statistical Associating Fluid Theory," Ind. Eng. Chem. Res., **54**(32), pp. 7942–7952.

[25] Hopp, M., and Gross, J., 2017, "Thermal Conductivity of Real Substances From Excess Entropy Scaling Using PCP-SAFT," Ind. Eng. Chem. Res., **56**(15), pp. 4527–4538.

[26] Schilling, J., Eichler, K., Kölsch, B., Pischinger, S., and Bardow, A., 2019, "Integrated Design of Working Fluid and Organic Rankine Cycle Utilizing Transient Exhaust Gases of Heavy-Duty Vehicles," Appl. Energy, **255**, p. 113207.

[27] White, M. T., Oyewunmi, O. A., Haslam, A. J., and Markides, C. N., 2017, "Industrial Waste-Heat Recovery Through Integrated Computer-Aided Working-Fluid and ORC System Optimisation Using SAFT-γ Mie," Energy Convers. Manage., **150**, pp. 851–869.

[28] Papaioannou, V., Lafitte, T., Avendaño, C., Adjiman, C. S., Jackson, G., Müller, E. A., and Galindo, A., 2014, "Group Contribution Methodology Based on the Statistical Associating Fluid Theory for Heteronuclear Molecules Formed From Mie Segments," J. Chem. Phys., **140**(5), p. 054107.

[29] White, M., Oyewunmi, O., Chatzopoulou, M., Pantaleo, A., Haslam, A., and Markides, C., 2018, "Computer-Aided Working-Fluid Design, Thermodynamic Optimisation and Thermoeconomic Assessment of ORC Systems for Waste-Heat Recovery," Energy, **161**, pp. 1181–1198.

[30] van Kleef, L. M., Oyewunmi, O. A., and Markides, C. N., 2019, "Multi-Objective Thermo-Economic Optimization of Organic Rankine Cycle (ORC) Power Systems in Waste-Heat Recovery Applications Using Computer-Aided Molecular Design Techniques," Appl. Energy, **251**, p. 112513.

[31] Aljundi, I. H., 2011, "Effect of Dry Hydrocarbons and Critical Point Temperature on the Efficiencies of Organic Rankine Cycle," Renewable Energy, **36**(4), pp. 1196–1202.

[32] Angelino, G., and Di Paliano, P. C., 1998, "Multicomponent Working Fluids for Organic Rankine Cycles (ORCs)," Energy, **23**(6), pp. 449–463.

[33] Chen, H., Goswami, D. Y., Rahman, M. M., and Stefanakos, E. K., 2011, "A Supercritical Rankine Cycle Using Zeotropic Mixture Working Fluids for the Conversion of Low-Grade Heat Into Power," Energy, **36**(1), pp. 549–555.

[34] Papadopoulos, A. I., Stijepovic, M., Linke, P., Seferlis, P., and Voutetakis, S., 2013, "Toward Optimum Working Fluid Mixtures for Organic Rankine Cycles Using Molecular Design and Sensitivity Analysis," Ind. Eng. Chem. Res., **52**(34), pp. 12116–12133.

[35] Rayegan, R., and Tao, Y., 2011, "A Procedure to Select Working Fluids for Solar Organic Rankine Cycles (ORCs)," Renewable Energy, **36**(2), pp. 659–670.

[36] Sauret, E., and Rowlands, A. S., 2011, "Candidate Radial-Inflow Turbines and High-Density Working Fluids for Geothermal Power Systems," Energy, **36**(7), pp. 4460–4467.

[37] Bahamonde, S., Pini, M., De Servi, C., Rubino, A., and Colonna, P., 2017, "Method for the Preliminary Fluid Dynamic Design of High-Temperature Mini-Organic Rankine Cycle Turbines," ASME J. Eng. Gas Turbines Power, **139**(8), p. 082606.

[38] Struebing, H., 2011, "Identifying Optimal Solvents for Reactions Using Quantum Mechanics and Computer-Aided Molecular Design," Ph.D. thesis, Imperial College London, London.

[39] Grossmann, I. E., Viswanathan, J., Vecchietti, A., Raman, R., and Kalvelagen, E., 2002, "GAMS/DICOPT: A Discrete Continuous Optimization Package," GAMS Development Corporation, Fairfax, VA.

[40] Floudas, C. A., 1995, Nonlinear and Mixed-Integer Optimization: Fundamentals and Applications (Topics in Chemical Engineering), Oxford University Press, New York.

[41] Adamczyk, J. J., 2000, "Aerodynamic Analysis of Multistage Turbomachinery Flows in Support of Aerodynamic Design," ASME J. Turbomach., **122**(2), pp. 189–217.

[42] Gross, J., 2005, "An Equation-of-State Contribution for Polar Components: Quadrupolar Molecules," AIChE J., **51**(9), pp. 2556–2568.

[43] Gross, J., and Vrabec, J., 2006, "An Equation-of-State Contribution for Polar Components: Dipolar Molecules," AIChE J., **52**(3), pp. 1194–1204.

[44] Stavrou, M., Lampe, M., Bardow, A., and Gross, J., 2014, "Continuous Molecular Targeting–Computer-Aided Molecular Design (CoMT–CAMD) for Simultaneous Process and Solvent Design for CO2 Capture," Ind. Eng. Chem. Res., **53**(46), pp. 18029–18041.

[45] Joback, K. G., and Reid, R. C., 1987, "Estimation of Pure-Component Properties From Group-Contributions," Chem. Eng. Commun., **57**(1–6), pp. 233–243.

[46] Ten, J. Y., Hassim, M. H., Chemmangattuvalappil, N., and Ng, D. K., 2016, "A Novel Chemical Product Design Framework With the Integration of Safety and Health Aspects," J. Loss Prev. Process Ind., **40**, pp. 67–80.

[47] De Servi, C., Campanari, S., Tizzanini, A., and Pietra, C., 2013, "Enhancement of the Electrical Efficiency of Commercial Fuel Cell Units by Means of an Organic Rankine Cycle: A Case Study," ASME J. Eng. Gas Turbines Power, **135**(4), p. 042309.

[48] Reynolds, W. C., and Colonna, P., 2017, Vapor Power Plants, Cambridge University Press, New York, Chap. 7.

[49] Glassman, A., 1976, "Computer Program for Design and Analysis of Radial Inflow Turbines," NASA, Lewis Research Center, Washington D.C., Report No. TN D-8164.

[50] Baines, N., 1998, "A Meanline Prediction Method for Radial Turbine Efficiency in Axial and Radial Turbines," Sixth International Conference on Turbocharging and Air Management Systems, London, Nov. 3–5, pp. 3–5.

[51] Pini, M., De Servi, C., Burigana, M., Bahamonde, S., Rubino, A., Vitale, S., and Colonna, P., 2017, "Fluid-Dynamic Design and Characterization of a Mini-Orc Turbine for Laboratory Experiments," Energy Procedia, **129**, pp. 1141–1148.

[52] Invernizzi, C., Iora, P., and Silva, P., 2007, "Bottoming Micro-Rankine Cycles for Micro-Gas Turbines," Appl. Therm. Eng., **27**(1), pp. 100–110.

[53] Benson, R. S., 1965, "An Analysis of the Losses in a Radial Gas Turbine," Proc. Inst. Mech. Eng., **180**(10), pp. 41–53.

[54] Persico, G., and Pini, M., 2016, "Fluid Dynamic Design of Organic Rankine Cycle Turbines," Organic Rankine Cycle (ORC) Power Systems: Technologies and Applications, E. Macchi, and M. Astolfi, eds., Woodhead Publishing, Cambridge, UK, pp. 253–297.

[55] Bülten, B., Althaus, W., Weidner, E., and Stoff, H., 2015, "Experimental and Numerical Flow Investigation of a Centripetal Supersonic Turbine for Organic Rankine Cycle Applications," 11th European Conference on Turbomachinery Fluid Dynamics and Thermodynamics, Madrid, Spain, March 23–25, pp. 23–27.

[56] Macchi, E., and Perdichizzi, A., 1981, "Efficiency Prediction for Axial-Flow Turbines Operating With Nonconventional Fluids," J. Eng. Power, **103**(4), pp. 718–724.

[57] Wiesner, F., 1967, "A Review of Slip Factors for Centrifugal Impellers," J. Eng. Power, **89**(4), pp. 558–566.

[58] Meitner, P. L., and Glassman, A. J., 1983, "Computer Code for Off-Design Performance Analysis of Radial-Inflow Turbines With Rotor Blade Sweep," NASA, Lewis Research Center, Washington D.C., Report No. NASA-E-1625.

[59] Casati, E., Colonna, P., and Nannan, N. R., 2011, "Supercritical ORC Turbogenerators Coupled With Linear Solar Collectors," ISES Solar World Congress 2011, Kassel, Germany, Aug. 28–Sept. 2, pp. 4056–4068.

[60] Xu, G., Song, G., Zhu, X., Gao, W., Li, H., and Quan, Y., 2015, "Performance Evaluation of a Direct Vapor Generation Supercritical ORC System Driven by Linear Fresnel Reflector Solar Concentrator," Appl. Therm. Eng., **80**, pp. 196–204.

[61] Li, C., Kosmadakis, G., Manolakos, D., Stefanakos, E., Papadakis, G., and Goswami, D., 2013, "Performance Investigation of Concentrating Solar Collectors Coupled With a Transcritical Organic Rankine Cycle for Power and Seawater Desalination Cogeneration," Desalination, **318**, pp. 107–117.

[62] Prabhu, E., 2006, "Solar Trough Organic Rankine Electricity System (Stores) Stage 1: Power Plant Optimization and Economics," U.S. National Renewable Energy Laboratory, Lakewood, CO Report No. NREL/SR-550-39433.

[63] Rohlik, H. E., 1968, "Analytical Determination of Radial Inflow Turbine Design Geometry for Maximum Efficiency," NASA, Lewis Research Center, Washington D.C., Report No. NASA-TN-D-4384.

[64] Whitfield, A., and Baines, N. C., 1990, Design of Radial Turbomachinery, Longman Scientific & Technical, Harlow, UK.

[65] Barr, L., Spence, S. W., and Eynon, P., 2008, "Improved Performance of a Radial Turbine Through the Implementation of Back Swept Blading," ASME Paper No. GT2008-50064.

[66] Di Bella, F. A., Di Nanno, L. R., and Koplow, M. D., 1983, "Laboratory and On-Highway Testing of Diesel Organic Rankine Compound Long-Haul Vehicle Engine," SAE Paper No. 830122.

[67] Brown, J. S., Brignoli, R., and Quine, T., 2015, "Parametric Investigation of Working Fluids for Organic Rankine Cycle Applications," Appl. Therm. Eng., **90**, pp. 64–74.

[68] Angelino, G., Invernizzi, C., and Macchi, E., 1991, "Organic Working Fluid Optimization for Space Power Cycles," Modern Research Topics in Aerospace Propulsion, G. Angelino, L. De Luca, and W. Sirignano, eds., Springer-Verlag, Berlin, pp. 297–326.

[69] Invernizzi, C. M., 2013, Closed Power Cycles (Lecture Notes in Energy, Vol. 11), Springer-Verlag, London.

[70] Ginosar, D. M., Petkovic, L. M., and Guillen, D. P., 2011, "Thermal Stability of Cyclopentane as an Organic Rankine Cycle Working Fluid," Energy Fuels, **25**(9), pp. 4138–4144.

[71] Invernizzi, C. M., Iora, P., Manzolini, G., and Lasala, S., 2017, "Thermal Stability of n-Pentane, Cyclopentane and Toluene as Working Fluids in Organic Rankine Engines," Appl. Therm. Eng., **121**, pp. 172–179.

[72] Invernizzi, C. M., and Bonalumi, D., 2016, "Thermal Stability of Organic Fluids for Organic Rankine Cycle Systems," Organic Rankine Cycle (ORC) Power Systems: Technologies and Applications, E. Macchi, and M. Astolfi, eds., Woodhead Publishing, pp. 121–151.

[73] Calderazzi, L., and Colonna di Paliano, P., 1997, "Thermal Stability of R-134a, R-141b, R-13I1, R-7146, R-125 Associated With Stainless Steel as a Containing Material," Int. J. Refrig., **20**(6), pp. 381–389.

[74] United Nations, 2017, "Economic Commission for Europe. Secretariat," Globally Harmonized System of Classification and Labelling of Chemicals (GHS), 7th ed., United Nations Publications, New York/Geneva.

[75] Chen, H., Goswami, D. Y., and Stefanakos, E. K., 2010, "A Review of Thermodynamic Cycles and Working Fluids for the Conversion of Low-Grade Heat," Renewable Sustainable Energy Rev., **14**(9), pp. 3059–3067.

[76] Eppinga, Q., Ganassin, S., and van Buijtenen, J., 2017, "Application and Operation of 40+ Triogen ORC Plants," Energy Procedia, **129**, pp. 684–691.

[77] Hawkins, L. A., Zhu, L., and Blumber, E. J., 2011, "Development of a 125 kW AMB Expander/Generator for Waste Heat Recovery," ASME J. Eng. Gas Turbines Power, **133**(7), p. 072503.